J Fluoresc (2008) 18:51–59
DOI 10.1007/s10895-007-0237-6

ORIGINAL PAPER

Effect of the Order and Disorder of $BaMoO_4$ Powders in Photoluminescent Properties

Ana Paula A. Marques · Francini C. Picon · Dulce M. A. Melo · Paulo S. Pizani · Edson R. Leite · José A. Varela · Elson Longo

Received: 17 January 2007 / Accepted: 7 August 2007 / Published online: 2 September 2007

Abstract The study of the photoluminescent properties affected by order and disorder of the $BaMoO_4$ powders is the principal objective in this work. $BaMoO_4$ compounds were prepared using soft chemical process called Complex Polymerization Method. In this work, different deagglomeration types and different heating rates were used to promote different disorder degrees. Scheelite type phase ($BaMoO_4$) was determined by X-ray Diffraction (XRD), Fourier Transformed Infra-Red (FTIR) and Raman spectroscopy after heat treating the sample at 400°C. The room temperature luminescence spectra revealed an intense single-emission band in the visible region. Based on XRD and Raman data it was observed that the transition between the completely disordered structure to completely ordered structure is a good condition for photoluminescence (PL) emission. The best PL emission is obtained when the material possesses short range disorder, i.e., is periodically ordered (XRD), but some disorder as measured by Raman spectroscopy. The excellent optical properties observed for disordered $BaMoO_4$ suggested that this material is a highly promising candidate for optical applications.

Keywords $BaMoO_4$ · Structural order-disorder · Complex polymerization method · Photoluminescence

A. P. A. Marques (✉) · F. C. Picon · E. R. Leite
LIEC-CMDMC, DQ, UFSCar,
Via Washington Luiz, Km. 235,
CEP 13565-905 São Carlos, SP, Brazil
e-mail: apamarques@liec.ufscar.br

D. M. A. Melo
Laboratório de Análise Térmica e Materiais, DQ, UFRN,
59072-970 Natal, RN, Brazil

P. S. Pizani
Laboratório de Semicondutores, DF, UFSCar,
Via Washington Luiz, Km. 235,
CEP 13565-905 São Carlos, SP, Brazil

J. A. Varela · E. Longo
LIEC-CMDMC, IQ, UNESP,
Rua Francisco Degni s/n,
CEP 14800-900 Araraquara, SP, Brazil

Introduction

$BaMoO_4$ (BMO) with a scheelite structure is an important material for applications in the industry due to its production of green luminescence and their approved usage as scintillating materials [1]. This compound has several applications, including solid-state lasers and optical fibers, being recently attracted great attention [2]. For one more comprehension of the luminescent properties of these type materials, several investigations have been carried out [2–7].

BMO have been produced by a variety of techniques that requires high temperatures or long reactions times [4, 8–10]. Inhomogeneous morphology and composition in BMO powders compounds would be relatively large because the MoO_3 has a tendency to vaporize at high temperatures [1]. For materials prepared by soft chemical process, such as the Complex Polymerization Method (CPM), these problems are reduced because the reaction occurs at lower temperature. Moreover the immobilization of metal-complexes in such rigid organic polymeric networks can reduce the segregation of particular metals, thus ensuring the compositional homogeneity at a molecular scale [5, 6, 11].

Numerous investigations have mentioned that the luminescent properties of materials like BMO are related to the structural order–disorder transformations. Several disordered compounds based on different metal oxianions with

intense PL at room temperature have been reported [12–14]. The coexistence of the localized levels and the polarization of the disordered materials can form several dynamic energy levels that act as optical absorption centers. These centers create favorable conditions to the luminescent emissions [13].

Considering that the CPM has been successful in preparing some oxide powders and that the structural order–disorder is related to the luminescent property, this work report the preparation of BMO by CPM, including your characterization, the dependence between the structural changes (disordered and ordered) and the photoluminescent properties.

Experimental

Materials

Molybdenum trioxide MoO_3 (Synth 85%), $BaCO_3$ (Mallinckrodt 99%), citric acid ($H_3C_6H_5O_7$) (Mallinckrodt 99%) and ethylene glycol ($HOCH_2CH_2OH$) (J. T. Baker 99%). All of the chemicals were used without further purification.

Synthesis

BMO was obtained by the CPM, in this synthesis the molybdenum citrate was prepared by the dissolution of MoO_3—molybdenum trioxide in an aqueous solution of citric acid under constant stirring at 60–80°C to homogenize the molybdenum citrate solution. The molar ratio between citric acid and total metallic cations was 6:1. After homogenization of this solution, barium precursor was dissolved and a stoichiometric amount added to the molybdenum citrate solution. Instead of solution to be clear and homogeneous instantaneity, the complex was well stirred for 2 h at 60–80°C. After the solution was homogenized, ethylene glycol was added to promote the citrate polymerization by the polyesterification. With continued heating at 80–90°C, the viscosity of the solution increased, albeit devoid of any visible phase separation. The molar ratio between barium and molybdenum cations was 1:1. The citric acid/ethylene glycol mass ratio was set to 60:40. After partial evaporation of the water, the resin was heat-treated at 300°C for 2 h, in a static atmosphere, leading to the partial decomposition of the polymeric gel, forming an expanded resin, constituted of partially pyrolyzed material (puff). The product was removed from the beaker and deagglomerated. The deagglomeration was done using a high energy milling. The powders were annealed at 400°C, 500°C, 600°C, and 700°C for 2 h in ambient atmosphere, with a heating rate of 10°C/min (BMO-10) and 5°C/min (BMO-5). These materials were compared to BMO powders obtained using mortar in the deagglomeration and a heating rate of 5°C/min [6].

Characterizations

The BMO sample pre-pyrolyzed were characterized by Termogravimetric analysis (TG) (STA 409, Netzsch, Germany) in synthetic air (100 cm^3/min) using a constant heating rate of 10°C/min. The evolution of the system with temperature was investigated by differential scanning calorimetry (DSC) (DSC 404C, Pegasus, Netzsch, Germany), in synthetic air (50 cm^3/min) using a constant heating rate of 1°C/min, 5°C/min, and 10°C/min from room temperature up to 1,000°C (DSC-1, DSC-5 and DSC-10, respectively).

The structural evolution and the unit cell volume of BMO powders were determined by X-ray diffraction (XRD) in a Rigaku Dmax2500PC diffractometer, using a Cu Kα radiation. The average crystallite diameter (D_{crys}) of the heat-treated powders was determined using the (112) diffraction peak (2θ around 26.5), according to the Scherrer equation (Eq. 1) [9]:

$$B = k \times \lambda / \left(D_{crys} \times \cos\theta\right), \quad (1)$$

where B is the full width at half maximum (FWHM), θ the Bragg angle, k is a constant and λ is the wavelength of the Cu Kα radiation.

The microstructure and surface morphology of the BMO crystalline powders heat-treated at 700°C were observed by High-Resolution Scanning Electron Microscopy (HR-SEM) using a Field Emission Gun–Supra35 Gemini-Zeiss equipment.

FTIR transmittance spectra of BMO were gathered in the frequency range of 400–2,100 cm^{-1} at room temperature using an Equinox/55 (Bruker) spectrometer. The Raman Spectroscopy data were obtained at room temperature using an RFS/100/S Bruker FT-Raman equipment with spectral

Table 1 Barium molybdate synthesis methods (BMO)

Method	Temperature (°C)	Time (h)	Synthesis products
Czochralski [8]	1,100–1,200	30–40	$BaMoO_4$
Spontaneous crystallization [4]	950	72	$BaMoO_4$
Calcination [9]	900	24	$BaMoO_4$
Calcination [10]	450	3	$BaMoO_4$, $BaO_2{\cdot}8H_2O$
$BaCl_2+Na_2MoO_4$ [15]	600	72	$BaMoO_4$
CPM, BMO-5[a]	400–500	2	$BaMoO_4$
CPM, BMO-10[a]	600	2	$BaMoO_4$

[a] The present work.

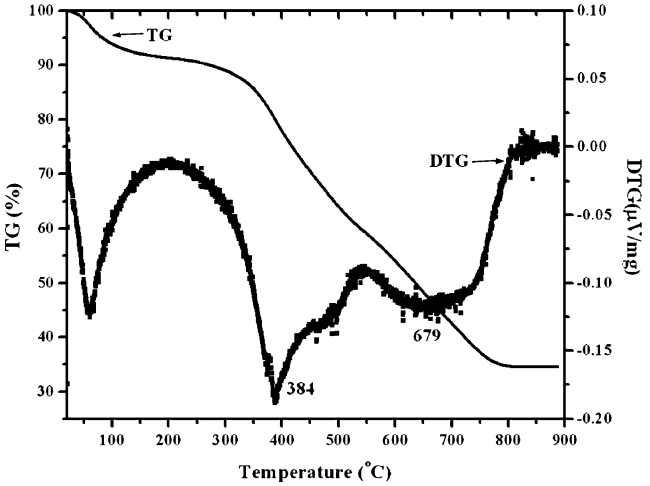

Fig. 1 TG/DTG curves of the BMO precursor in synthetic air, using a constant heating rate of 10°C/min

resolution of 4 cm^{-1} attached to a Nd:YAG laser promoting an excitation light of 1064 nm, in the frequency range of 100–1,000 cm^{-1}.

PL spectra of BMO powders were collected with a U1000 Jobin–Yvon double monochromator coupled to cooled GaAs photomultiplier and a conventional photon counting system. The 488.0 nm exciting wavelength of an argon ion laser was used. The maximum output power of the laser was 20 mW. All measurements were taken at room temperature.

Results and discussion

Several methods are described for the synthesis of the BMO powders where high temperature and long reaction time are required as shown in Table 1 [4, 6, 8–10, 15]. BMO has a scheelite crystal structure with tetragonal symmetry (β) C^6_{4h} at room temperature. The phase transition to cubic structure (α) takes place at 1,873°C [8]. Due to this phase transition, the preparation of single crystal requiring a high tempera-

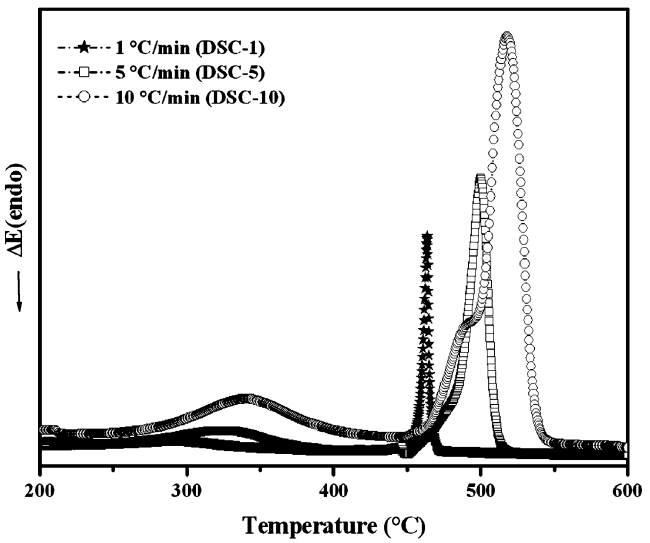

Fig. 2 DSC curves of the BMO precursor in synthetic air, using a constant heating rate of 1°C/min (DSC-1), 5°C/min (DSC-5), and 10°C/min (DSC-10)

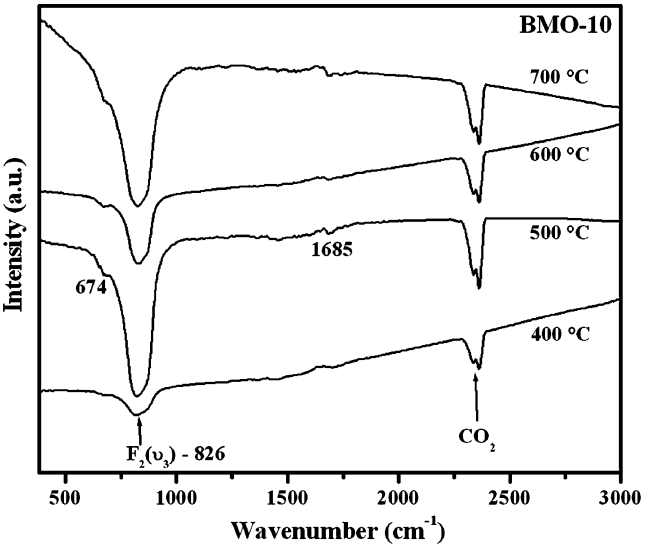

Fig. 3 FTIR absorption spectra of the BMO-10 heat-treated at 400°C, 500°C, 600°C, and 700°C

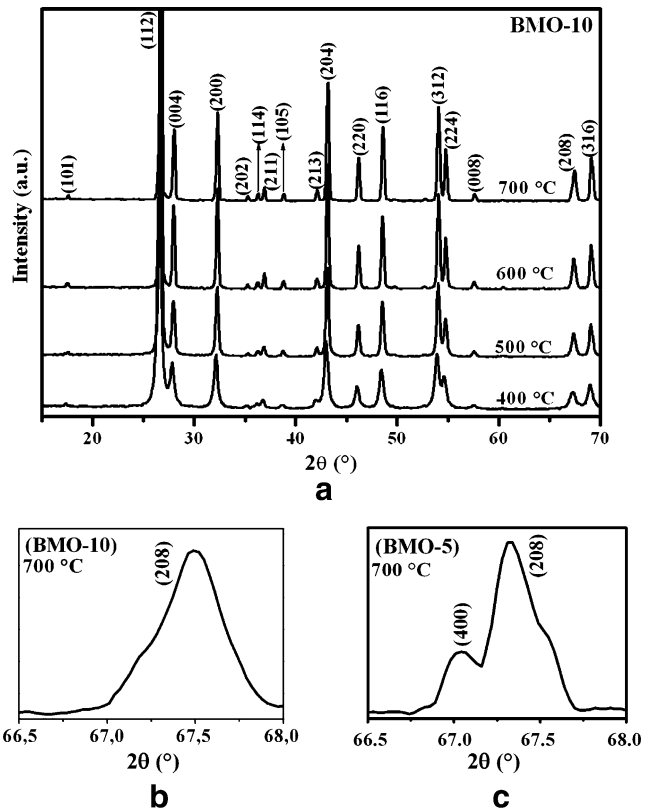

Fig. 4 **a** XRD patterns of the BMO-10 powders calcined at various temperatures: 400°C, 500°C, 600°C, and 700°C (15–70°), **b** the BMO-10 heat-treated at 700°C (66.5–68.0°), and **c** the BMO-5 heat-treated at 700°C (66.5–68.0°)

Table 2 Crystallite sizes and lattice constants of the tetragonal structure of BMO powders prepared by the CPM method and heat-treated at different temperatures

Sample BMO (°C)	Crystallite sizes (nm)	Lattice constants (Å)	
		a	*c*
400	29 (±1.4)	5.571 (2)	12.815 (6)
500	34 (±1.7)	5.564 (1)	12.802 (5)
600	45 (±2.3)	5.562 (1)	12.799 (6)
700	45 (±2.2)	5.572 (4)	12.780 (20)

ture can be quite difficult. In this work, the temperature used is low (approximately 550°C) and the reaction time is short (2 h). Furthermore, the reaction products do not present any additional phase.

Figure 1 shows the TG/DTG curves in a synthetic air atmosphere for the decomposition of BMO sample pre-pyrolyzed (300°C for 2 h). The thermogravimetric analysis (TGA curve) of the materials shows about three decomposition stages. The TGA indicated a minor weight loss (8%) between 50°C and 100°C, what corresponds to the evaporation of absorbed water and other residual organics, followed by a weight loss (15%) between 100°C and 390°C, which is probably due to the decomposition of polymeric chain and elimination of CO_2 and H_2O. The major weight loss (36%) occurs between 390°C and 800°C referent to elimination of carbonates linked with Mo. After 800°C, no obvious weight loss was observed.

Figure 2 shows the Differential Scanning Calorimetry (DSC) curves of the BMO pre-pyrolyzed; this data was collected using three different constant heating rates, 1°C/min (DSC-1), 5°C/min (DSC-5) and 10°C/min (DSC-10). Figure 2 shows that the exothermic peak of DSC-1 appears in temperature minor and more defined that DSC-5 and DSC-10. The fast heating tends to reduce the resolution of the curve but increases the peak area and the temperature at which the peak appears (the "peak position"). Superheating and runaway exothermic reactions are more likely to occur at fast heating rates (DSC-10). Slow heating tends to give small peaks areas if there is good thermal contact between the sample and the heating block [16]. This results indicating that the crystallization temperature phase scheelite in the DSC-1 starts before and that the process occurs with minor zone of temperature that DSC-5 and DSC-10, respectively. In DSC-1 and DSC-5 appear only one exothermic peak at 463°C and 498°C, respectively, attributed to the crystallization temperature of the scheelite phase. The DSC-10 presented two overlapped exothermic peaks (491°C and 518°C). The first process, with a peak at 491°C can be attributed to the formation of the disordered phase of BMO, and, the second process, with a peak at 518°C, is attributed to the crystallization temperature of the scheelite phase [17]. The exothermic peaks before that 400°C (DSC-1, DSC-5 and DSC-10) are relatives to the decomposition of polymeric chain and elimination of CO_2 and H_2O.

Figure 3 present the FTIR spectra of the BMO heat-treated at 400–700°C, with a heating rate of 10°C/min. FTIR spectrum of BMO shows that all compounds have tetrahedral symmetry. The representation for tetrahedral symmetry is: $\Gamma_{Td}=A_1(\nu_1)+E(\nu_2)+F_2(\nu_3)+F_2(\nu_4)$, but only the $F_2(\nu_3, \nu_4)$ modes are active in the IR spectrum. The $F_2(\nu_3)$ vibrations are the antisymmetric stretches, and the $F_2(\nu_4)$ vibrations are bending modes. Nakamoto [18] shows that the υ(CO) stretching occurs at 2375–1,100 cm^{-1} and the υ(OCO) stretching occurs at 1,100–550 cm^{-1}. In the BMO FTIR spectrum of the vibration around 1,685 cm^{-1} is attributed to the asymmetric vibration of COO. The bands around 670 and 674 cm^{-1} are attributed to the υ(OCO) stretching. For higher temperature treatment, more organic components are eliminated and more carbon-free intermediate inorganic disordered phase is added, and consequently, the stretching related to the organic components is less intense. The spectra of the BMO displayed a very broad absorption band in the range of 820 to 830 cm^{-1}. These bands are assigned to $F_2(\nu_3)$ antisymmetric stretch vibrations, which were reported to be ascribed to the Mo–O stretching vibration in MoO_4^{2-}. These bonds present well definition with increasing calcining temperature. This fact probably occurs because increasing calcining temperature the crystalline structure is increasingly ordered and this band shows a better definition, a characteristic confirmed by XRD and Raman spectroscopy.

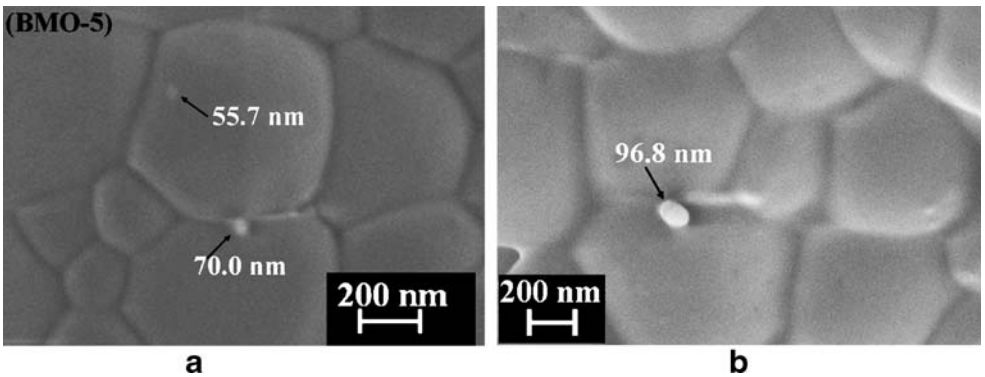

Fig. 5 **a** HR-SEM micrograph of BMO-5 and **b** BMO-10 powders heat-treated at 700°C for 2 h

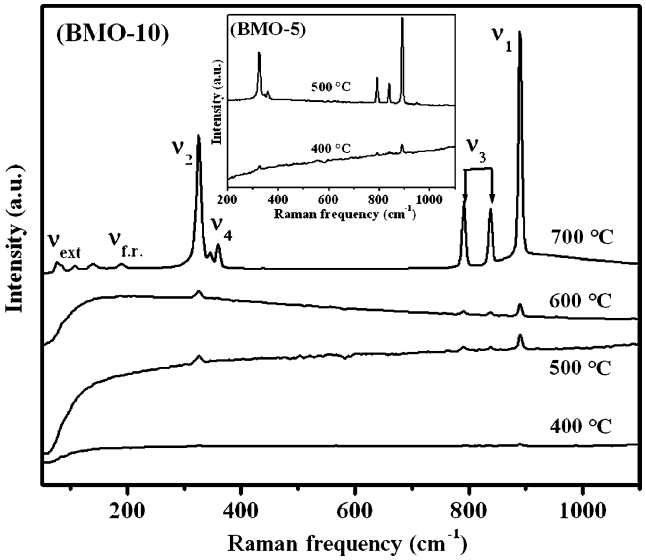

Fig. 6 Spontaneous Raman spectra of BMO-10 powders heat-treated at 400°C, 500°C, 600°C, and 700°C and BMO-5 powders heat-treated at 400°C and 500°C

The XRD patterns of the BMO powders heat-treated at different temperatures are shown in Fig. 4. The BMO calcined at 400°C for 2 h was crystalline, displaying scheelite type phases, but with broader Bragg reflection than those observed to material treated at higher temperatures [3, 15, 19, 20; JCPDS No. 29-0193]. All diffraction peaks were indexed according to the JCPDS data base (JCPDS No. 29-0193) and pointed to the tetragonal symmetry. The CPM was shown to be efficient for this synthesis, as it allowed to synthesize BMO powders displaying the scheelite (β) structure.

From the peak positions displayed in Fig. 4, the lattice parameters were calculated using the least square refinement from the REDE93 program. The lattice parameters a and c for these BMO powders are similar to those values reported for bulk material (a=5.5802 Å and c=12.8210 Å) (JCPDS No. 29-0193). Table 2 present the lattice parameters a and c and the mean crystallite sizes for the BMO powders heat-treated at different temperatures, with a heating rate of 5°C/min (BMO-5) and 10°C/min (BMO-10). The calculated mean crystallite sizes of BMO heat-treated at temperatures ranging from 400°C to 700°C increase with the calcining temperature reaching value of 45 nm at 700°C for both BMO synthesized.

Figure 5 presents a HR-SEM micrograph of BMO powders deagglomerated using a high energy milling and heat-treated at 700°C for BMO-5 and BMO-10. In this figure it was observed that both BMO presents an agglomerate of individual particles, with size about 602 and 659 nm, respectively. This result was very different to BMO powders heat-treated in the same temperature, 700°C, with a heating rate of 5°C/min, however using mortar in a deagglomeration. The BMO using mortar showed an agglomerate of individual particles, whose crystallite sizes are around of 40–50 nm [6]. The difference in mean particle size observed certainly is due to deagglomeration-procedure used. The deagglomeration using high energy milling provokes steps in the surface of particles. This process of steps in particle surface probable provokes the growth of grain contours, favoring the sintering process and consequently the higher crystallite size [21]. Figure 5 show small particles (around of 60 nm) and higher particles (around of 600 nm), this observation indicate that small particles coalesce into large particles forming big ones. These observations indicate that crystallite sizes calculated form XRD data cannot correspond to real particle size.

The spontaneous Raman spectra with the assignments of the BMO-10 Raman-active vibration modes are presented Fig. 6 and detailed in Table 3. The BMO unit cell includes two formula units, $[MoO_4]^{2-}$ ionic group and the Ba^{2+}

Table 3 Raman mode frequencies for the BMO powders heat-treated at different temperatures

Lattice mode symmetry $C^6_{4\,h}$	BMO-5		BMO-10	BMO[a]	Assignments
	700°C	600°C	700°C	1100–1200°C	
A_g	891	890	890	892	ν_1 (A_1)
B_g	838	838	838	837	ν_3 (F_2)
E_g	791	791	791	791	
E_g	359		359	358	ν_4 (F_2)
B_g	346		346	345	
B_g	326	325	326	324	ν_2 (E)
A_g	325	325	325	324	
E_g	190		187	188	$\nu_{f.r.}$ (F_1)—free rotation
B_g	141		139	137	$\nu_{ext.}$—external modes MoO_4^{2-} and Ba^{2+} motions
E_g	107		108	110	
B_g	78		81	76	
E_g	76		76	74	

[a] Czocharalski method [1].

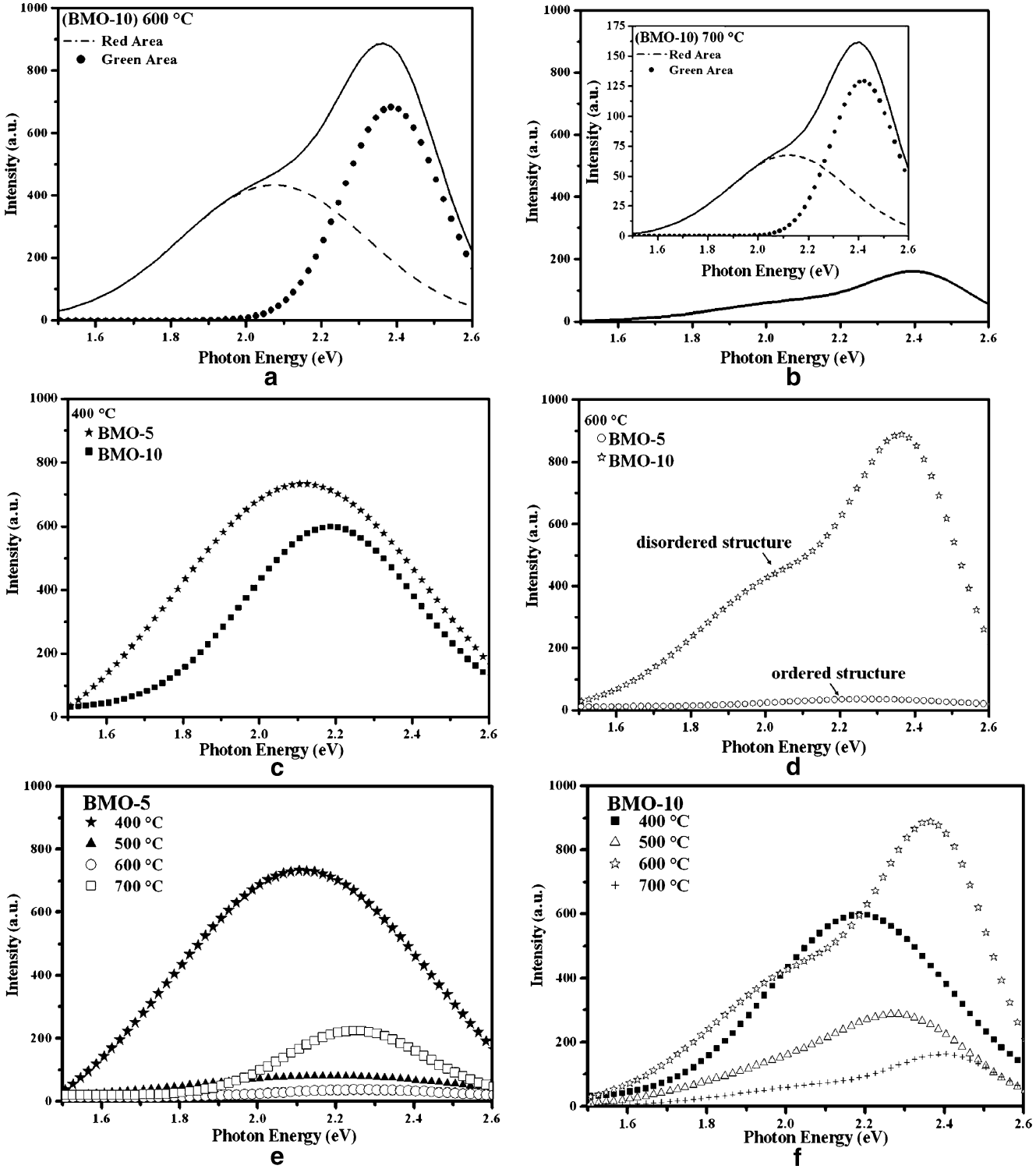

Fig. 7 Room temperature PL spectra of BMO excited with the 488 nm line of an argon ion laser: **a** BMO-10 heat-treated at 600°C for 2 h, **b** BMO-10 heat-treated at 700°C for 2 h, **c** BMO-5 and BMO-10 heat-treated at 400°C for 2 h, **d** BMO-5 and BMO-10 heat-treated at 600°C for 2 h, **e** BMO-5 heat-treated at 400°C, 500°C, 600°C, and 700°C for 2 h, and **f** BMO-10 heat-treated at 400°C, 500°C, 600°C, and 700°C

cations [8]. The $[MoO_4]^{2-}$ ionic group, peculiar to the BMO scheelite structure, have strong covalent Mo–O bonds. Due to weak coupling between the $[MoO_4]^{2-}$ ionic group and the Ba^{2+} cations, the vibrational modes observed in the spontaneous Raman spectra of BMO scheelite crystals can be divided into two groups, internal and external modes. The internal mode correspond to the vibrations within the $[MoO_4]^{2-}$ group, with an immovable

mass center (ν_1, ν_2, ν_3, and ν_4). The external or lattice phonons correspond to the motion of the Ba^{2+} cations and the rigid molecular unit. $[MoO_4]^{2-}$ tetrahedral in free space have T_d-symmetry (ν_{ext}).

The Raman spectra showed the well-resolved sharp peaks for the BMO-10 powders treated at 700°C, indicating that the synthesized powders were highly crystallized. The Raman spectra of BMO-10 heat-treated at 400°C and 500°C do not present such well-resolved sharp peaks, but their crystallizations were observed by XRD. In BMO-10 treated at 600°C main sharp peaks are present, displaying only internal modes, so, it is ordered at short distance. This disagreement among XRD and Raman data occurs probably because the materials are disordered at middle distance with defects that are periodically repeated at long distance.

According to quantum confinement theory, the energy band gap of a semiconductor depends on the crystal size; its value will increase with a decrease in crystal size. Minor energy band gap favors the photoluminescence (PL) properties. Consequently, can be correct expected that the PL properties increase with the increase of the treatment temperature. However, other variables can be studied. Figure 7 illustrates the photoluminescence (PL) spectra recorded at room temperature for the BMO-10 and BMO-5 heat-treated at different temperatures, for 2 h. The samples were excited by the 488 nm line of an argon ion laser. The photoluminescence emission characteristics were broad and intense bands. The PL emission spectra could be decomposed into two Gaussian-shaped curves, ascribed to red–yellow and green emission bands. According to Orhan et al. [12], the emission photoluminescent in scheelite type materials is due to structural disorder in the MoO_4 cluster, which is caused by the displacement of the one of these oxygens, changing the bond length. So, the red–yellow and green components of the band can be ascribed to:

MoO_4–O–MoO_3 red and yellow;
MoO_4–O–MoO_3 green.

The PL intensity and the band emission wavelength depend on the thermal treatment history of the powders, and therefore, to their structural order. In this work, it was observed that the BMO samples presented small variations in relative areas of both red–yellow and green peaks. In spite of small variation in relative area, these results are in agreement with the work of Marques et al. [5, 6], in which the BMO thin film and nanopowders with the highest PL intensity possessed the biggest red–yellow area.

The red–yellow band (peak 1) represents, respectively, 56%, 46%, 55% and 50% of the total PL band area for BMO-10 heat-treated at 400°C to 700°C for 2 h, respectively (see Table 4). The BMO-10 sample that presented the smallest PL intensity was the one heat-treated at 700°C for 2 h. Their PL emission areas are equally distributed in the both regions, indicating that different emissions compete for the PL intensity. The decomposition of the overall PL emission spectra indicates that the fraction of PL emission ascribed to the green emission band increases with the structural disorder degree, as pointed by Marques et al. [5, 6] and Orhan et al. [12, 13]. It is evident the dislocation of the PL to green region for BMO-10 sample heat-treated at 600°C compared to the BMO-10 heat-treated at 400°C (more disordered). However, the contribution of red–yellow emission is still bigger, than green emission in the PL band.

Table 4 Evolution of the red PL fraction with the structural order (BMO)

Samples	BMO-5			BMO-10		
	Peak 1[a]	Peak 2[a]	RA/FA	Peak 1[a]	Peak 2[a]	RA/FA
400°C/2 h	1.99	2.32	0.65	2.04	2.30	0.56
500°C/2 h	1.92	2.34	0.54	2.03	2.31	0.46
600°C/2 h	1.90	2.44	0.49	2.07	2.39	0.55
700°C/2 h	2.01	2.32	0.26	2.10	2.42	0.50

RA: area of the red decomposed band, *FA*: area of the fitted band
[a] United in eV.

Raman spectroscopy is an effective tool for studying the effects of structural disorder. For a perfect crystal the first-order Raman phonon spectrum consists of narrow lines that correspond to Raman-allowed zone center (Γ-point) modes, which obey definite polarization selection rules. For the case of disordered crystals, however, the following features are anticipated in the phonon spectrum: (1) a broadening of the first-order Raman lines; (2) The activation of forbidden Raman phonons; (3) appearance of broad Raman bands reflecting the phonon density of states; (4) frequency shifting of some peaks proportional to the concentration of the dopant element (i.e., one-phonon-like behavior), and (5) splitting of some peaks involving different elements that share the same lattice site (i.e., two-phonon-like behavior) [22]. As observed in Fig. 6, the order at short distance in BMO-10 started at 700°C and BMO-5 is ordered when the sample is heat-treated at 500°C.

XRD data (Fig. 4) shows that both samples are periodically ordered after heat treatment for temperature above 400°C, because the Bragg reflection display scheelite type phase. Nevertheless, the BMO-10 difratogram shows broader Bragg reflection, which demonstrates more disorder in this system compared with BMO-5, that present fine Bragg reflection. The Bragg reflection for the plane (400) occurs for BMO-5, but not for BMO-10, indicating that BMO-5 is more ordered than BMO-10 at 700°C.

Based on the XRD and Raman data it is possible to conclude that the PL emission is related to partially ordered structure. BMO-10 samples heat-treated at 400°C is totally

disordered and PL emission observed in this condition is very small. Otherwise, BMO-5 sample heat-treated at this temperature displays some diffraction peaks referent to crystalline structure, as shown in XRD, but is disordered at short range, as shown by Raman data (Fig. 6). The PL of BMO-5 sample heat-treated at 400°C is higher compared with BMO-10 sample heat-treated in the same temperature (see Fig. 7c).

Increasing calcining temperature for both samples to 500°C result in decrease of PL intensity for both samples, being very sharp for BMO-5 sample. In this calcining temperature BMO-5 sample is ordered whereas the BMO-10 sample is disordered at short range. Increasing the calcining temperature for both samples to 600°C causes long range order for sample BMO-5 leading to practically no PL emission. However the sample BMO-10 is more disordered at short range and displays the best PL emission. Both samples calcined at 700°C practically displays no PL emission due to long and short range order acquired for both samples.

In this way it is possible to conclude that the PL property is directly related to the order–disorder of the material. The best PL emission occurs when the material is disordered at short range (Raman) but possesses periodic order (XRD), that is, possess order at long range.

This disorder at short range is determined by the calcining temperature and by heating rate. This work shows that the material heat-treated with low heating rate (5°C/min) promotes long range order at 500°C, whereas for material with higher heating rate the long range order is promoted only at 700°C. Then, using heating rate of 10°C/min leads to low ordering of the material promoting disordered states (short range) which is favorable for PL property.

Conclusion

BMO crystalline scheelite type phases could be identified in BMO powder prepared by the CPM method after calcining at 400°C.

The deagglomeration of BMO powder using high energy milling promotes steps on the particle surface that probably promotes growth of grain contours, favoring the sintering process and consequently the higher crystallite size of BMO.

The PL property observed in this material is directly related to order–disorder. The best PL emission occurs when the material is disordered at middle range (Raman) but not at long range (XRD), that is, possess periodic order. In this work the material heat-treated with low heating rate (5°C/min) promotes long range order at 500°C whereas for material with higher heating rate (10°C/min) the long range order is promoted only at 700°C. Then, using heating rate of 10°C/min leads to low ordering of the material promoting disordered states (middle range) which is favorable for PL property.

The excellent optical properties observed for disordered BMO suggested that this material is a highly promising candidate for photoluminescent applications.

Acknowledgements The authors gratefully acknowledge FAPERN, FAPESP-CEPID, CNPq, and CAPES. The authors gratefully acknowledge Miryam R. Joya of the Departamento de Fisica, Universidade Federal de São Carlos for collaborating in this article by accomplishing the measures of PL.

References

1. Cho WS, Yashima M, Kakihana M, Kudo A, Sakata T, Yoshimura M (1997) Active electrochemical dissolution of molybdenum and the application for room-temperature synthesis of crystallized luminescent calcium molybdate film. J Am Ceram Soc 80(3):765–769
2. Cho WS, Yoshimura M (1997) Preparation of highly crystallized $BaMoO_4$ film using a solution reaction assisted by electrochemical dissolution of molybdenum. Solid State Ion 100(1–2):143–147
3. Ryu JH, Yoon JW, Lim CS, Oh WC, Shim KB (2005) Microwave-assisted synthesis of $CaMoO_4$ nano-powders by a citrate complex method and its photoluminescence property. J Alloys Compd 390(1–2):245–249
4. Spassky DA, Ivanov SN, Kolobanov VN, Mikhailin VV, Zemskov VN, Zadneprovski BI, Potkin LI (2004) Optical and luminescent properties of the lead and barium molybdates. Radiat Meas 38(4–6):607–610
5. Marques APA, de Melo DMA, Longo E, Paskocimas CA, Pizani PS, Leite ER (2005) Photoluminescence properties of $BaMoO_4$ amorphous thin films. J Solid State Chem 178:2346–2353
6. Marques PA, de Melo DMA, Paskocimas CA, Pizani PS, Joya MR, Leite ER, Longo E (2006) Photoluminescent $BaMoO_4$ nanopowders prepared by complex polymerization method (CPM). J Solid State Chem 179:658–665
7. Mikhrin SB, Mishin AN, Potapov AS, Rodnyi PA, Voloshinovskii AS (2002) X-ray excited luminescence of some molybdates. Nucl Instrum Methods Phys Res Sect A Accel Spectrom Detect Assoc Equip 486(1–2):295–297
8. Basiev TT, Sobol AA, Voronko YuK, Zverev PG (2000) Spontaneous Raman spectroscopy of tungstate and molybdate crystal for Raman lasers. Opt Mater 15:205–216
9. Hitoki G, Takata T, Ikeda S, Hara M, Kondo JN, Kakihana M, Domen K (2000) Mechano-catalytic overall water splitting on some mixed oxides. Catal Today 63(2–4):175–181
10. Hasan MA, Zaki MI, Kumasi K, Pasupulety L (1998) Soot deep oxidation catalyzed by molybdena and molybdates: a thermogravimetric investigation. Thermochim Acta 320(1–2):23–32
11. Maurera MAMA, Souza AG, Soledade LEB, Pontes FM, Longo E, Leite ER, Varela JA (2004) Microstructural and optical characterization of $CaWO_4$ and $SrWO_4$ thin films prepared by a chemical solution method. Mater Lett 58:727–732
12. Orhan E, Anicete-Santos M, Maurera MAMA, Pontes FM, Souza AG, Andrès J, Bèltran A, Varela JA, Pizani PS, Taft CA, Longo E (2005) Towards an insight on the photoluminescence of disordered $CaWO_4$ from a joint experimental and theoretical analysis. J Solid State Chem 178(4):1284–1291
13. Orhan E, Anicete-Santos M, Maurera MAMA, Pontes FM, Paiva-Santos CO, Souza AG, Varela JA, Pizani PS, Longo E (2005) Conditions giving rise to intense visible room temperature

photoluminescence in $SrWO_4$ thin films: the role of disorder. Chem Phys 312(1–3):1–9
14. Leite ER, Pontes FM, Lee EJH, Aguiar R, Longo E, Pontes DSL, Nunes MSJ, Macedo R, Pizani PS, Lanciotti F Jr, Boschi TM, Varela JA, Paskocimas CA (2002) A novel approach for the development of photoluminescent material. Appl Phys A Mater Sci Process 74(4):529–532
15. Nassif V, Carbonio RE (1999) Neutron diffraction study of the crystal structure of $BaMoO_4$: a suitable precursor for metallic $BaMoO_3$ perovskite. J Solid State Chem 146(1):266–270
16. Daniels TC (1973) Thermal analysis. Wiley, New York, p 99
17. Pontes FM, Leite ER, Nunes MSJ, Pontes DSL, Longo E, Magnani R, Pizani PS, Varela JA (2004) Preparation of $Pb(Zr,Ti)O_3$ thin films by soft chemical route. J Eur Ceram Soc 24(10–11):2969–2976
18. Nakamoto K (1986) Infrared and Raman spectra of inorganic and coordination compounds (4th ed). Wiley, New York
19. Xia T, Fuenzalida VM, Zarate RA (2001) Electrochemical preparation of crystallized $Ba_{1-x}Sr_xMoO_4$ solid-solution films at room-temperature. J Alloys Compd 316(1–2):250–255
20. Thangadurai V, Knittlmayer C, Weppner W (2004) Metathetic room temperature preparation and characterization of scheelite-type ABO_4 (A=Ca, Sr, Ba, Pb; B=Mo, W) powders. Mater Sci Eng B Solid-State Mater Adv Technol 106(3):228–233
21. Kingery WD (1957) Ceramic fabrication processes. MIT Press, Cambridge
22. Moura MR, Ayala AP, Guedes I, Grimsditch M, Loong C-K, Boatner LA (2004) Raman scattering study of $Tb(V_{1-x}P_x)O_4$ single crystals. J Appl Phys 95(3):1148–1151